Estimation of Threshold Age for Cerebral Decline Using Sigmoidal Growth Model in Cross-Sectional Imaging Study

Namhee Kim *, Moonseong Heo, Roman Fleysher, Malka Z. Sears, Michael L. Lipton

Posted Date: 18 September 2023

doi: 10.20944/preprints202309.1143.v1

Keywords: aging; sigmoidal growth function; nonlinear regression; threshold estimation; fractional anisotropy

Article

Estimation of Threshold Age for Cerebral Decline Using Sigmoidal Growth Model in Cross-Sectional Imaging Study

Namhee Kim [1]*, Moonseong Heo [2], Roman Fleysher [3], Malka Zughaft Sears and Michael L. Lipton [3,4]

[1] Rush Alzheimer's Disease Center, Rush University Medical Center, Chicago, IL, 60612, USA
[2] Department of Public Health Sciences, Clemson University, South Carolina, SC, 29634, USA
[3] Department of Radiology, Columbia University Irving Medical Center, New York, NY, 10032, USA
[4] Department of Biomedical Engineering, Columbia University, New York, NY, 10027, USA
* Correspondence: namhee_kim@rush.edu

Abstract: Backgrounds: Linear association has widely been assumed for prediction of aging-related fractional anisotropy (FA) decline in white matter of the brain. While useful for testing significance of the aging effect, it fails to identify a threshold age before and after which the age-FA association changes. Identification of such a threshold is often of clinical interest for timely intervention. **Methods:** We employed a sigmoidal growth function to test a threshold effect in age triggering onset of cerebral decline in 21 white matter tracts, and compared its fitting performance to those of linear, and power regression. The study sample was a normal healthy cohort of 106 participants with ages in mid-life ranging from 18 to 60 years. **Results:** Of the 21 white matter tracts analyzed, the posterior thalamic radiation showed better fit with sigmoidal curve model, compared to a linear or power regression. The estimated threshold age in years (95% confidence interval) were 47.2 (44.1-48.4). **Conclusion:** While available evidence regarding the presence of a specific age threshold for cerebral decline in mid-life based on FA was limited, the posterior thalamic radiation exhibited a threshold age of 47.2. Beyond this age point, we observed a significant change in the FA risk pattern.

Keywords: aging; sigmoidal growth function; nonlinear regression; threshold estimation; fractional anisotropy

1. Introduction

Even normal aging is associated with changes in the microstructural composition of white matter (WM), partly attributed to loss of myelin (1, 2) . Loss of myelin facilitates directional heterogeneity of water diffusion compared to densely myelinated WM where diffusion is highly constrained to predominantly parallel to the axis of axon bundles. Microstructural changes in myelin density can thus be indexed as a decrease in fractional anisotropy (FA) from Diffusion Tensor Imaging (DTI).

In almost all diffusion magnetic resonance imaging (MRI) studies, analytic approaches have sought linear relationships between FA and age, often quantified by linear regression coefficients or correlations. While those association measures are straightforward to compute, and useful for identifying significant risk factors, they fail to identify a threshold beyond which an abrupt change in risk pattern is expected. Estimating a threshold age beyond which senescent epochs in lifespan defined by the pattern of FA as function of age begins could add information regarding the aging process and enhance clinical relevance of neuroimaging measures. Of the few studies that have applied non-linear approaches to this issue, Kochunov et al. (1) used a second order polynomial regression to identify such a threshold age. Once a threshold age was determined, a linear regression on age was then fitted to each epoch, before and after the threshold, in a piece-wise linear regression fashion. Brickman et al. (3) also applied a linear regression to fit FA during each epoch after identifying a threshold age by visual inspection of the data.

Sigmoidal curves, S- or inverse S-shaped, are frequently used for fitting or modeling biological data (4-7). A special feature of the sigmoidal growth function is its ability to model a threshold (7), where the rate of change (i.e., the first derivative of the curve) reaches the maximum at the threshold

Preprints (www.preprints.org) | NOT PEER-REVIEWED | Posted: 18 September 2023 doi:10.20944/preprints202309.1143.v1

and vanishes at both extremes on the X-axis. This particular feature is different from those of both piece-wise linear regression approaches, described above, which assume a symmetric and constant rate of change within each epoch before and after the threshold.

Our prior study (7) examined the threshold effect of cumulative heading exposure among amateur soccer players; where heading is a putative risk factor for low FA. We fitted FA data by adopting sigmoidal growth curve and estimated a threshold exposure level where risk for low FA increased. The study showed the FA pattern was sharply split into two segments separated by the estimated threshold; FA leveled off in both tail areas of the two segments of heading exposure.

Building upon our prior study (7), we aimed to estimate a threshold age for abrupt FA changes across a young to middle aged segment of the adult lifespan, by applying the sigmoidal growth functions to a total of 21 white matter tracts, including projection, limbic, association, and callosal fibers. The list of 21 WM tracts is presented in Supplementary material S1. We hypothesize that there exists a threshold age at which FA begins to decline, consistent with onset of subclinical senescence in the mid-life years (18-60) as studied in (1, 3). Confirmation of this hypothesis would indicate that FA trends or trajectories across the lifespan may be more complicated than the continuous decline assumed by a single linear or simple sequence of two linear associations separated by a threshold age, as was assumed in prior studies of age-related white matter change.

We review the sigmoidal growth model in Section 2.1 and then present alternative models for comparison in Section 2.2, followed by a description of DTI data acquisition and preprocessing in Section 2.3. Analysis results based on sigmoidal growth function are presented in Section 3, followed by discussion and conclusion in Section 4 and 5.

2. Materials and Methods

2.1. Sigmoidal Growth Function Regression Model

Sigmoidal growth model has been widely adopted to describe the biological, pharmacological dynamics of dose-response curve (4-7). The general form of sigmoidal growth function is based on a logistic regression model and written as follows.

$$y_i = f(x_i, \mathbf{z}_i) = \boldsymbol{\alpha}'\mathbf{z}_i + \frac{\beta_1}{1+\exp\left(-\beta_2 (x_i - \beta_3)\right)} + e_i \qquad (1)$$

where $\mathbf{z}_i$ represents covariates, $\boldsymbol{\alpha}$ is the coefficients of $\mathbf{z}_i$, and x_i is the variable of interest explored for its threshold effect; here, x_i represents age of the i-th participant. We impose a positive constraint on β_2 so that β_2 (> 0) solely determines the rate change of the exponential curve. Let us define $g(x) = f(x;\mathbf{z}) - \boldsymbol{\alpha}'\mathbf{z}$. Since $\lim_{x\to-\infty} g(x) = 0$ and $\lim_{x\to\infty} g(x) = \beta_1$, β_1 determines the scale (or maximum) of the curve as well as its shape, S-shape ($\beta_1 > 0$) or inverse S-shape ($\beta_1 < 0$). Change in outcome y_i in Model (1) at an x is determined by the first derivative of f with respect to x, that is,

$$\frac{\partial f}{\partial x} = \beta_2 g(x)\left(1 - \frac{1}{\beta_1} g(x)\right) \qquad (2)$$

The greatest absolute change (slope) of f occurs when x is equal to β_3, where the first derivative function at $x = \beta_3$ in Equation (2) ($= \frac{\partial f}{\partial x}(\beta_3;\mathbf{z}) = \beta_1\beta_2/4$) takes the maximum if $\beta_1 > 0$ and the minimum if $\beta_1 < 0$. Thus β_2 determines the change of f at the threshold (or inflection) point β_3, and a larger value of β_2 represents a sharper transition of y at β_3.

The nonlinear sigmoidal growth function in Model (1) can be fitted by iterative nonlinear least square optimization algorithms such as Gauss-Newton and Levenberg-Marquardt algorithm (8-10). We used the latter algorithm since it provides better convergence due to its flexible step size at each

 doi:10.20944/preprints202309.1143.v1

iteration (8). To avoid local maximums, we used 100 different sets of starting values of parameters and then selected the parameter set that maximizes the log-likelihood function value. We use a likelihood ratio test (LRT) to test significance of parameters since LRT is robust to potentially non-symmetric sampling distribution of the parameter estimates and small samples compared with other tests such as a Wald test as demonstrated in (11, 12). Details of nonlinear regression and LRT are demonstrated in Supplementary material S2 and S3.

2.2. Linear and Power Regression Models

The following alternative models were compared to the sigmoidal growth function (Model (1)):

$$y = \boldsymbol{\alpha}'\mathbf{z} + \beta_1 x^{\beta_2} + e \tag{3}$$

$$y = \boldsymbol{\alpha}'\mathbf{z} + \beta_1 x + e \tag{4}$$

where $\mathbf{z}_i$ represents covariates as before, $\boldsymbol{\alpha}$ is the coefficients of $\mathbf{z}_i$. Model (3) is a power regression model of x whereas Model (4) is a simple linear regression; of note, the linear model is a reduced form of the Model (3) when $\beta_2 = 1$. Since the power regression model shown in Model (3) is again nonlinear function of x, the Levenberg-Marquardt algorithm for nonlinear least square optimization is employed. These two competing models are not nested within the sigmoidal growth function in Model (1), however.

We adopt three model selection criteria Mean Squared Error (MSE), Akaike Information Criteria (AIC) and Bayesian Information Criterion (BIC) for choosing the optimal model across the three competing models, (1), (3) and (4). All models were fitted and tested using MATLAB and SAS.

2.3. DTI Acquisition and Preprocessing

DTI was performed using a 3.0 T MRI scanner (Achieva; Philips Medical Systems, Best, The Netherlands) with an eight-channel head coil (Sense Head Coil; Philips Medical Systems). T1-weighted whole-head structural imaging was performed using sagittal three-dimensional magnetization-prepared rapid acquisition gradient echo (MP-RAGE; TR/TE/TI = 9.9/4.6/1250 msec; field of view, 240 mm^2; matrix, 240 × 240; and section thickness, 1 mm). T2-weighted whole-head imaging was performed using axial two-dimensional turbo spin-echo (TR/TE = 4000/100 msec; field of view, 240 mm^2; matrix, 384 × 512; and section thickness, 2 mm). DTI was performed using single-shot echo-planar imaging (TR/TE = 11000/51 msec; field of view, 240 mm^2; matrix, 120 × 120; section thickness, 2 mm; independent diffusion sensitizing directions, 32; and b = 800 s/mm^2).

FA was derived from DTI at each voxel using the FMRIB Diffusion Toolbox (13). Preprocessing procedures implemented for DTI included skull stripping, echo-planar imaging distortion correction, intermediate rigid-body registration, registration to standard space, transformation of DTI to standard space, and white matter segmentation, in sequence. Non-brain voxels were removed from the MP-RAGE and turbo spin-echo images using FMRIB-FSL software (14). Each brain volume was inspected section-by-section, and residual non-brain voxels were removed manually. Turbo spin-echo images were acquired with the same section thickness, position and orientation as DTI. Distortion correction was accomplished using a nonlinear deformation algorithm to match each echo-planar image to the corresponding turbo spin-echo volumes (15). For intermediate rigid-body registration, each subject's turbo spin-echo images were registered to their three-dimensional MP-RAGE volume using the Automated Registration Toolbox (ART) (16) three-dimensional rigid-body approach (17). For registration to standard space, the nonlinear registration module in ART was used to register each subject's three-dimensional MP-RAGE volume to a standard T1-weighted template, the Johns Hopkins University (JHU) T1 (JHU-MNI-SS-T1) (18, 19). For transformation of DTI to the standard space, distortion correction, intermediate rigid-body registration, and standard space registration were applied to the calculated FA maps in a single resectioning operation using ART. Final cubic voxel size was 1 mm^3, masked to exclude non-brain voxels from the analysis. For white

Preprints (www.preprints.org) | NOT PEER-REVIEWED | Posted: 18 September 2023 doi:10.20944/preprints202309.1143.v1

matter segmentation, the fast automated segmentation tool in the FMRIB-FSL package (14) was used to generate a white matter mask for the three-dimensional MP-RAGE template brain images and restrict subsequent statistical analysis of FA to white matter voxels. Details of DTI preprocessing were described previously (20). A JHU-MNI-SS atlas (JHU-MNI-SS-WMPM-Type-II) with comprehensive WM parcellation (19) was used to extract WM anatomical information from each co-registered individual FA volume. Mean FA was obtained from each of the 21 WM tracts delineated by the JHU atlas in each hemisphere for each participant.

2.4. Participants

A total 106 healthy participants, 34 women and 72 men, with ages ranging from 18 to 60 years, and with no history of medical, neurological or psychiatric disease were enrolled in a study addressing normal variation of brain imaging measures in healthy individuals across the lifespan between August 2010 and May 2015. All studies were approved by an Institutional Review Board of Albert Einstein College of Medicine. Written informed consent was obtained from each participant.

3. Results

To estimate threshold ages where the rate of FA decline changes, the sigmoidal growth function in Model (1) as well as the two competing models (3) and (4) were fitted to the mean FA from each of the 21 WM fiber tracts. Among the 21 tracts examined, a linear association between FA and age was prevalent, evidenced by 11 WM tracts displaying lower MSE, 18 tracts with lower AIC, and 20 tracts with lower BIC when using a linear model. However, one specific WM tract, the posterior thalamic radiation, exhibited a notable threshold effect of age on FA that shows the lowest MSE, AIC, and BIC with the sigmoidal growth function (Table 1). The three competing models were also compared in terms of MSE, AIC, and BIC for all 21 WM tracts as presented in Supplementary material S4.

Table 1. Comparison of fitting performances from three competing models.

The posterior thalamic radiation	MSE	AIC	BIC
Sigmoidal growth model	640.0	991.7	1005.0
Power model	686.7	998.1	1008.8
Linear model	692.3	997.0	1005.0

Note: MSE: Mean square error; AIC: Akaike Information Criterion; BIC: Bayesian Information Criterion.

The final sigmoidal function fitted to the posterior thalamic radiation was estimated as

$$f(x) = \beta_0 + \beta_1 \Big/ \left(1 + \exp\left(-\beta_2 \left(x_{age} - \beta_3\right)\right)\right),$$

where $\hat{\beta}_0$ = 496.7, $\hat{\beta}_1$ = -37.1, $\hat{\beta}_2$ = 5.7, and $\hat{\beta}_3$ = 47.2. Specifically, the estimated threshold age (β_3) was 47.2 years with 95% C.I. of [44.1, 48.4] ($p < 0.0001$) for the posterior thalamic radiation (Table 2). The scale factor of the curve (β_1) was negative, and thus the estimated curve is an inverse S-shape (p-value = 0.00002). We note that testing for the null hypothesis (β_2) , which is that rate of change of the sigmoidal curve at the threshold age is not necessary, since β_2 is constrained to be positive as mentioned in Section 2.1. The fitted sigmoidal growth function (Model (1)) with its 95% prediction intervals for the posterior thalamic radiation tract is presented in Figure 1 (a), and those from two competing models (linear & power model) in Figure 1 (b).

Table 2. Hypothesis test on the significance of a threshold age: $H_0 : \beta_3 = 0$.

	Estimate	95% CI	P-value
The posterior thalamic radiation	47.2	(44.1, 48.4)	<0.0001

Preprints (www.preprints.org) | NOT PEER-REVIEWED | Posted: 18 September 2023 doi:10.20944/preprints202309.1143.v1

Lastly, the sigmoidal growth function assumes that FA levels off in the tails of both epochs. For this reason, a response pattern either gradually decreasing or increasing in each epoch may not be detected. Therefore, we examined the significance of such a potential lack-of-fit by applying linear regressions for each epoch and tested the significance of the coefficient of age (H_0: $\gamma=0$). Results showed that no significant linear associations of FA with age were found in the posterior thalamic radiation for the epochs before (E_{before}) and after (E_{after}) the threshold age (γ = -0.36, p=0.36, n=87 in E_{before}; γ = -0.19, p=0.89, n=19 in E_{after}).

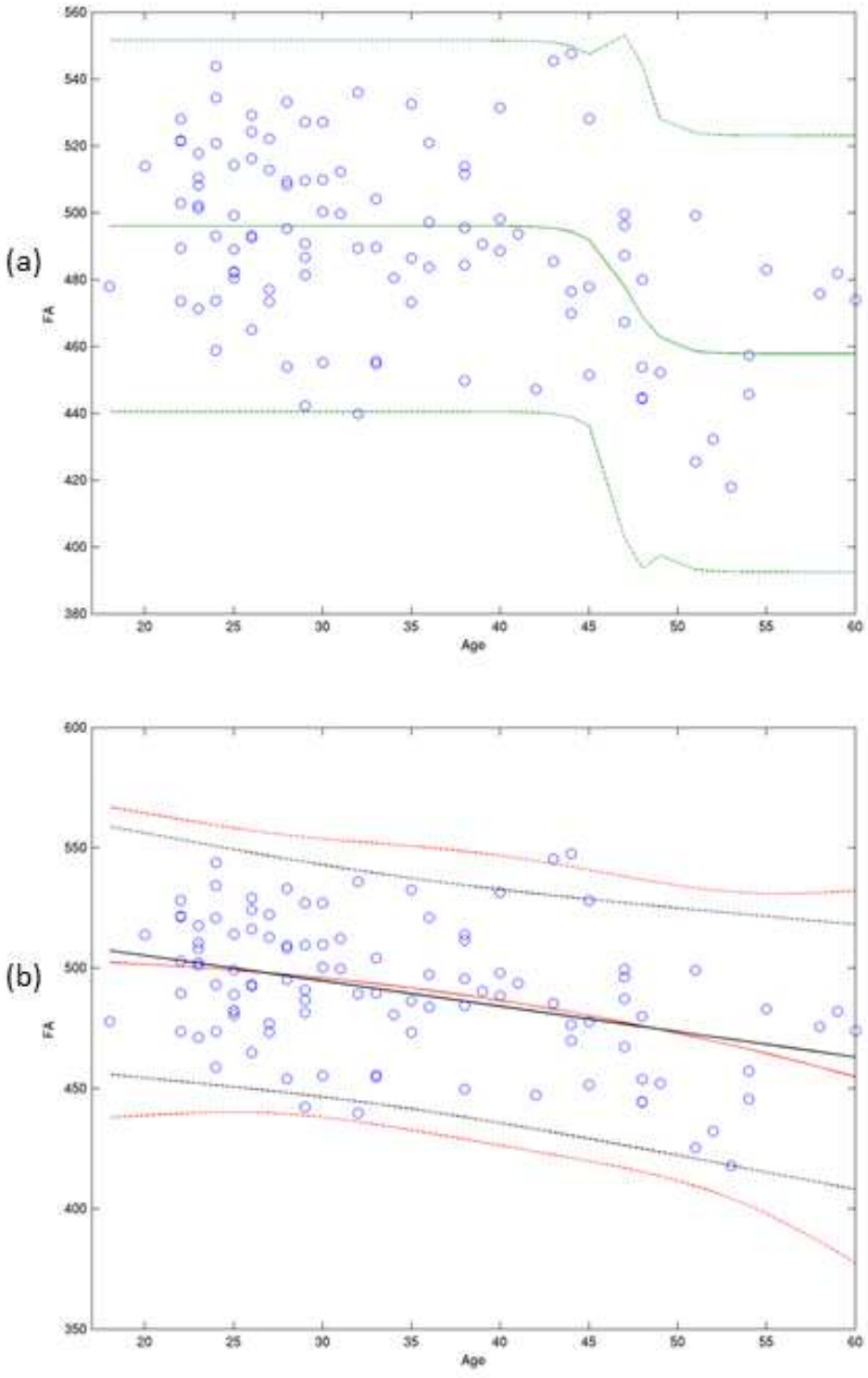

Figure 1. Modeling Growth Patterns for the Posterior Thalamic Radiation Tract. Figure 1. a) presents a sigmoidal growth function (represented by the green solid line) along with its corresponding 95%

 doi:10.20944/preprints202309.1143.v1

prediction interval (shown as green dotted lines) fitted for the posterior thalamic radiation. Similarly, in Figure 1(b), we have fitted both a power function (red solid line) and a linear model (black line) along with their respective 95% prediction intervals (red and black dotted lines, respectively).

4. Discussion

In a cohort of healthy young to middle aged adults (18-60 years) we find that in the posterior thalamic radiation, the associations between age and FA may not be a linear, but more likely follow the pattern of a step function, where FA levels are different before and after a threshold age.

Kochunov (1) estimated the threshold separating maturation and senescence to be around 32 years (32 ± 6) for 9 white matter tracts in 831 healthy participants aged 11 to 90. This threshold varied across the tracts and extended into the 3rd and 4th decades of life. Similarly, Brickman (3) suggested 30 years as a threshold by visually inspecting data from the cerebral peduncle and the posterior limb of the internal capsule in 282 healthy participants aged 7 to 87 years. Our study found a different estimated age threshold, 47.2 years, for the posterior thalamic radiation, which exceeds the range of threshold ages suggested in previous studies (1, 3). Notably, the age spectrum covered in the previous two studies was extensive, encompassing individuals from adolescence through the final decade of life (7 to 90 years). The primary emphasis of these studies was to estimate the age at which peak myelin maturation occurs, expected to be during the transition from youth to mid-life. In contrast, our study focused on identifying the threshold age for senescent changes in mid-life.

We tested the effect of sex by including sex-specific intercepts in the sigmoidal growth function in Model (1) as a covariate, and found that it is not significant (data not shown). Different threshold age effect by sex was tested by fitting a separate sigmoidal growth curve for each sex group. Sex-specific 95% CI's for the estimated threshold age were overlapped (data not shown). We surmise that testing the of sex effect would require a larger cohort for more accurate assessment of difference in sex-specific threshold ages.

Optimization of nonlinear power regression with a WM track (Tapatum) failed to converge with all 100 sets of starting values described in Section 2.2. These failures are suspected to be attributed to a couple of reasons. Firstly, Tapatum represents a relatively small region within the white matter, making the reliable estimation of FA a challenging task. Alternatively, it could be linked to over-parameterization, where certain parameters within the nonlinear functions in Models (1) and (6) become redundant, resulting in the singularity of the Jacobian matrix.

We strictly compared competing model performance using penalized model comparison criteria (AIC and BIC) to prevent overfitting. The sigmoidal curve performed better with the posterior thalamic radiation than linear and power regression model in terms of MSE and AIC, however, it was tied with linear model in terms of BIC, the most stringent criteria for model selection. Therefore, we conclude that the sigmoidal model with the posterior thalamic ration attains both the lowest MSE and the highest parsimony among the three tested models.

We observed a significant age-related threshold effect on fractional anisotropy (FA), particularly within the posterior thalamic radiation at around the age of 47. Thalamocortical radiations are bundles of nerve fibers that establish connections between the thalamus and the cerebral cortex. Specifically, the posterior thalamic radiation connects the thalamus to the parietal and occipital lobes, facilitating the transmission of input from the eyes and other sensory modalities (21-23). The American Optometric Association (AOA) reports that starting in the early to mid-40s, many adults may experience difficulties with clear vision in their daily lives (source: https://www.aoa.org/healthy-eyes/eye-health-for-life/adult-vision-41-to-60-years-of-age?sso=y). Age-related changes in vision first manifest in alterations related to the projection of light onto the retina, followed by processing in the early levels of the cerebral visual cortex to detect simple features such as orientation and contrast, and subsequently progress to higher-level visual processing (24). A future study is warranted to gain a better understanding of the changes occurring in the cerebral visual cortex through changes in the posterior thalamic radiation.

This study has several limitations. Since lower FA is thought to indicate microstructural change that leads to cognitive decline, it will be important to examine whether individuals beyond the threshold age also exhibit cognitive decline and whether the degree of cognitive decline is associated with the degree of decline in FA. Addressing these important questions will require longitudinal follow-up of individuals, which is beyond the scope of the present study. Analysis of an expanded age span may require more flexible models that allow for the presence of multiple thresholds for both epochs. To this end, larger sample sizes are warranted for more accurate estimation of model parameters and fuller characterization of FA changes with normal aging.

5. Conclusion

A sigmoidal growth curve better characterized aging-related FA decline of the posterior thalamic radiation. While linear or quadratic models have usually been adopted to estimate the trajectory of FA over the lifespan, our study suggests aging-related FA trajectory in mid-life could be far from such simple patterns. Therefore, FA trajectories across the lifespan could be more complicated than a single linear or simple sequence of two piecewise linear associations separated by a threshold age.

Supplementary Materials: The following supporting information can be downloaded at the website of this paper posted on Preprints.org.

Authors Contribution NK designed the study, conducted data analysis, and prepared a draft. RF and ML designed DTI protocol. ML and MZ recruited study participants. RF and ML acquired DTI data. RF conducted DTI data preprocessing. MH, RF, MS, and ML provided critical reviews, corrections and revisions. All authors read and approved the final version of the manuscript.

Funding This work was supported by The Dana Foundation, David Mahoney Neuroimaging Program and by NIH: R01 NS082432, R01AG015819, R01AG17917, R01AG056405, R01AG059732, P30AG072975, R01AG075728, and R01AG055430.

Ethics and Consent Participants were recruited through advertisements in the local urban community (Bronx, NY) after Albert Einstein College of Medicine Institutional Review Board (IRB) approval. All participants gave written informed consent.

Data availability. The dataset supporting the conclusions of this article will be included in an additional file. Please visit the RADC Research Resource Sharing Hub (www.radc.rush.edu) to obtain data for research purposes.

Competing Interests The authors declare that they have no competing interests.

References

1. Kochunov P, Williamson DE, Lancaster J, Fox P, Cornell J, Blangero J, Glahn DC. Fractional anisotropy of water diffusion in cerebral white matter across the lifespan. *Neurobiol Aging.* 2012 Jan; 33(1): 9-20. PMCID: PMC2906767.
2. Xiong YY, Mok V. Age-related white matter changes. *J Aging Res.* 2011; 2011: 617927. PMCID: PMC3163144.
3. Brickman AM, Meier IB, Korgaonkar MS, Provenzano FA, Grieve SM, Siedlecki KL, Wasserman BT, Williams LM, Zimmerman ME. Testing the white matter retrogenesis hypothesis of cognitive aging. *Neurobiol Aging.* 2012 Aug; 33(8): 1699-1715. PMCID: PMC3222729.
4. Tsoularis A, Wallace J. Analysis of logistic growth models. *Math Biosci.* 2002; 179(1): 21-55.
5. Lefkovitch LP. The study of population growth in organisms grouped by stages. *Biometrics.* 1965: 1-18.
6. Caglar MU, Teufel AI, Wilke CO. Sicegar: R package for sigmoidal and double-sigmoidal curve fitting. *PeerJ.* 2018 Jan 16; 6: e4251. PMCID: PMC5774301.
7. Lipton ML, Kim N, Zimmerman ME, Kim M, Stewart WF, Branch CA, Lipton RB. Soccer heading is associated with white matter microstructural and cognitive abnormalities. *Radiology.* 2013 Sep; 268(3): 850-857. PMCID: PMC3750422.
8. Seber G, Wild CJ. Nonlinear regression. New York Wiley; 1989.
9. Bates DM, Watts DG. Nonlinear regression analysis and its applications. New York: Wiley; 1988.
10. Levenberg K. A method for the solution of certain non-linear problems in least squares. *Quarterly of Applied Mathematics.*

11. Pastor R, Guallar E. Use of two-segmented logistic regression to estimate change-points in epidemiologic studies. *Am J Epidemiol.* 1998 Oct 1; 148(7): 631-642.
12. Agresti A. An introduction to categorical data analysis. New York: A Wiley-Interscience publication; 1996.
13. Smith SM, Johansen-Berg H, Jenkinson M, Rueckert D, Nichols TE, Miller KL, Robson MD, Jones DK, Klein JC, Bartsch AJ, Behrens TE. Acquisition and voxelwise analysis of multi-subject diffusion data with tract-based spatial statistics. *Nat Protoc.* 2007; 2(3): 499-503.
14. Smith SM, Jenkinson M, Woolrich MW, Beckmann CF, Behrens TEJ, Johansen-Berg H, Bannister PR, De Luca M, Drobnjak I, Flitney DE, Niazy RK, Saunders J, Vickers J, Zhang Y, De Stefano N, Brady JM, Matthews PM. Advances in functional and structural MR image analysis and implementation as FSL. *Neuroimage.* 2004; 23 Suppl 1: 208.
15. Lim KO, Ardekani BA, Nierenberg J, Butler PD, Javitt DC, Hoptman MJ. Voxelwise correlational analyses of white matter integrity in multiple cognitive domains in schizophrenia. *Am J Psychiatry.* 2006 Nov; 163(11): 2008-2010. PMCID: PMC1950260.
16. Ardekani BA, Braun M, Hutton BF, Kanno I, Iida H. A fully automatic multimodality image registration algorithm. *J Comput Assist Tomogr.* 1995; 19(4): 615-623.
17. Ardekani BA, Guckemus S, Bachman A, Hoptman MJ, Wojtaszek M, Nierenberg J. Quantitative comparison of algorithms for inter-subject registration of 3D volumetric brain MRI scans. *J Neurosci Methods.* 2005 Mar 15; 142(1): 67-76.
18. Holmes CJ, Hoge R, Collins L, Woods R, Toga AW, Evans AC. Enhancement of MR images using registration for signal averaging. *J Comput Assist Tomogr.* 1998; 22(2): 324-333.
19. Oishi K, Faria A, Jiang H, Li X, Akhter K, Zhang J, Hsu JT, Miller MI, van Zijl PC, Albert M, Lyketsos CG, Woods R, Toga AW, Pike GB, Rosa-Neto P, Evans A, Mazziotta J, Mori S. Atlas-based whole brain white matter analysis using large deformation diffeomorphic metric mapping: Application to normal elderly and alzheimer's disease participants. *Neuroimage.* 2009 Jun; 46(2): 486-499. PMCID: PMC2885858.
20. Lipton ML, Kim N, Park YK, Hulkower MB, Gardin TM, Shifteh K, Kim M, Zimmerman ME, Lipton RB, Branch CA. Robust detection of traumatic axonal injury in individual mild traumatic brain injury patients: Intersubject variation, change over time and bidirectional changes in anisotropy. *Brain Imaging Behav.* 2012 Jun; 6(2): 329-342.
21. Ouyang Y, Cui D, Yuan Z, Liu Z, Jiao Q, Yin T, Qiu J. Analysis of age-related white matter microstructures based on diffusion tensor imaging. *Front Aging Neurosci.* 2021 Jun 28; 13: 664911. PMCID: PMC8273390.
22. Aeby A, Liu Y, De Tiège X, Denolin V, David P, Balériaux D, Kavec M, Metens T, Van Bogaert P. Maturation of thalamic radiations between 34 and 41 weeks' gestation: A combined voxel-based study and probabilistic tractography with diffusion tensor imaging. *AJNR Am J Neuroradiol.* 2009 Oct; 30(9): 1780-1786. PMCID: PMC7051519.
23. Neuroanatomy, thalamocortical radiations [homepage on the Internet]. StatPearls Publishing. 2023 Jul 24,. Available from: https://www.ncbi.nlm.nih.gov/books/NBK546699/.
24. Andersen GJ. Aging and vision: Changes in function and performance from optics to perception. *Wiley Interdiscip Rev Cogn Sci.* 2012 May; 3(3): 403-410. PMCID: PMC3424001.
25.